Published in final edited form as:
J Magn Reson. 2013 August ; 233: 103–106. doi:10.1016/j.jmr.2013.05.012.

Non-cryogenic ultra-low field MRI of wrist-forearm area

I. Savukov, **T. Karaulanov**, **C. Wurden**, and **L. Schultz**
Los Alamos National Laboratory

Abstract

Ultra-low field (ULF) MRI as an alternative to high field MRI can find some niche applications where high field is a liability. Previously we demonstrated hand images with a non-cryogenic ULF MRI system, but such a system was restrictive to the size of the imaging objects. We have modified the previous setup to increase the imaging volume and demonstrate the image of human hand near the wrist area. One goal for the demonstration is the evaluation of quality of larger bone structure to project image quality to other parts of extremities, such as elbows, shoulders, knees, etc. We found that after 12 minutes of acquisition the image quality was quite satisfactory. To achieve this image quality, several problems were solved that appeared in the new system. The increase in the imaging volume size led to an increase in transient time and various measures were taken to reduce this time. We also explored a method of overcoming the artifacts and image quality reduction arising from field drifts present in the system due to heating of the coils. We believe that our results can be useful for evaluation of diagnostic capability of non-cryogenic ULF MRI of extremities and other parts of the body. The system can be also applied to image animals and tissues.

Keywords

Ultra-low field; anatomical; imaging; low-cost; portable; alternative MRI

I. Introduction

The image quality of MRI (i.e., resolution and signal-to-noise ratio [SNR]) improves with the strength of the magnetic field, and currently high-field (3T) MRI provides state-of-the-art image quality. However, some disadvantages of high-field MRI include: high cost, high field, heavy weight, large size, etc. The problem of high cost is partially resolved with mid- and low-field MRI scanners (0.1-1 T). These scanners also have an open design that facilitates MRI applications with claustrophobic patients and children requiring parental assistance. In addition, image contrast improves at low fields [1], susceptibility artifacts are reduced enabling imaging patients with metal implants [2], the RF power decreases, which eliminates the danger of burns, and the acoustical noise level is reduced. Although these advantages are important, the crucial factor is the clinical relevance. Despite the loss of SNR and resolution, low- and mid-field scanners are still quite efficient in the diagnosis of diseases [4-8].

Further reduction in price, weight, size, energy consumption and improvement in portability and contrast [9] can be achieved with ultra-low field (ULF) scanners based on the pulsed

pre-polarization method designed to partially compensate for loss of signal. Most recently, high quality images of extremities using strong pre-polarization field (0.4 T) were demonstrated [10,11] – these images rival high field systems in sensitivity and resolution. Various features of the low-field approach such as absence of susceptibility artifacts [11,12] and nitrogen dips were also demonstrated [11,13]. However, this system has not yet been developed into a large-size imager.

While many pre-polarized MRI experiments have been based on pick-up coils, to improve the sensitivity in the ULF regime superconducting quantum interference devices (SQUIDs) have also been employed [14]. SQUIDs brought the advantage of non-resonant multi-channel operation [15]. SQUIDs have been used to demonstrate the detection of explosives in airport [16] and anatomical imaging of the brain combined with MEG [17].

To avoid cryogenics, atomic magnetometers (AMs) have been tested as detectors for ULF NMR [18] and MRI [19,20]. To reduce the cost and complexity of the AM and to accommodate sufficient bandwidth for MRI, it is necessary to raise the NMR frequency to 100 kHz and above. An AM sensitivity of 0.24 $fT/Hz^{1/2}$ was demonstrated at 423 kHz [21] for NQR, and such a sensitivity is sufficient for good quality imaging. However, unlike NQR detection, NMR detection with AM has some difficulties. One difficulty is that the AM and NMR fields have to be different by 3 orders of magnitude. A long solenoid was tested in [22] for field separation, but this solution is far from ideal: the field is not sufficiently uniform inside the solenoid, the imaging objects are restricted, and a large gradient that is applied during the MRI measurement time would broaden the AM resonance and decrease its sensitivity. Alternatively, a flux-transformer (FT) has been used to transfer the NMR signal to the AM. MRI relevant to clinical imaging was demonstrated with this approach [20]. Unfortunately the non-cryogenic FT introduces substantial Johnson noise, 1-10 $fT/Hz^{1/2}$. However, this noise can be reduced by increasing frequency. We used an RF shield made of copper to reduce noise from the large pre-polarization coil and environment. The RF shield is also a source of Johnson noise, but this noise is also mitigated by using higher Larmor frequency [23]. Smaller coils and multi-channel systems can provide additional advantage in the sensitivity. The advantage of the AM+FT configuration is the possibility to run multi-channel acquisition to improve SNR [20] and reduce dramatically time required for the scan.

To investigate the performance and noise of a ULF-MRI system with a pre-polarization coil and internal shield we developed a non-cryogenic pick-up coil based hand-MRI ULF scanner operating at 83.6 kHz [24]. We demonstrated hand-MRI imaging with 2×2 and 1.5×1.5 mm^2 resolutions acquired in less than 20 minutes. To improve sensitivity we used a specialized coil with high filling fraction and used a small-size pre-polarization (Bp) coil. The significance of this effort was the demonstration of ULF-MRI on a very small scale without cryogens or bulky shielding. However, this system was quite restrictive for the imaged objects. For example, it did not allow us to image various parts of the hand or the arm. For many applications, it would be necessary to develop a system with larger imaging volume and convenient access. In particular, the imaging of the wrist, forearm, and elbow is needed in many medical applications. MRI scanning of arm parts is an important diagnostic procedure to determine a number of anomalies such as abscesses, bursitis, bone fractures, ganglion cyst, bone infection, injuries of tendon, ligaments, tumors, etc. Most critical anomalies have relatively large size [25] and can be detected with even low-resolution MRI (~2-3 mm); hence ULF MRI can be of practical interest for this. It also has been shown that ULF MRI has enhancement of contrast for various anomalies as expected from larger differences in relaxation rates at ULF [1].

Our new modified system for hand and arm imaging has many parts identical to those used in the previous setup [24], namely, the Bm and gradient coils, the gradient amplifiers, computer interface, but several parts such as the Bp coil, the switch for the Bp coil, the rf shield, and the pick-up coil were replaced. The sequence also was the same, although the sequence parameters were optimized for new conditions. The MRI signal is detected with a saddle pick-up coil, resonated with a capacitor, and connected to an amplifier. In more detail the system is described next.

II. Method

To increase the volume for imaging we modified significantly our previous setup [24] used for the hand MRI. First of all, we increased the dimensions of the Bp electro-magnet to an ID of 160 mm and a depth of 190 mm. Second, we replaced the previous detection and excitation coils with larger saddle coils that allow the insertion of the forearm. The RF excitation coil (ID=122 mm) was slightly larger than the receiver coil (ID=100mm) and was oriented perpendicular to reduce transients and noise arising from the amplifier driving the RF coil. The receiver and excitation coils were shielded from the Bp coil by a relatively long aluminum cylindrical shell (ID=148 mm, thickness 2 mm, length 230 mm) with a disc cap at one end. The shell was connected to the amplifier ground to reduce rf interference noise. The receiver coil was made smaller than the shield to decrease the transmission of thermal noise from the shield. This noise and the internal Johnson noise of the coil are limiting factors for sensitivity. Ambient magnetic-field gradients were compensated for with the gradient coils.

To compensate for the loss of sensitivity of the new larger receiver coil compared to the previous side-solenoid [24], we doubled the pre-polarization field. This was achieved by increasing the power by a factor of four and rebuilding the Bp switch. To facilitate winding and to lower the voltage of the power supply to a safe level, the Bp electromagnet was made from four equal coils. Each Bp coil was driven individually by an electronic switch connected to a separate power supply. Switches were made by combining multiple commercial solid-state switches to increase maximum current. Some additional circuits were added to protect the switches against large voltages generated during Bp switch-off.

The increase in the size and the field strength of the Bp coil system resulted in longer transients, not only in the Bp coils but also in the parallel and hence inductively coupled Bm coil. The transients in the Bm coil were reduced from 100 ms to 60 ms by driving it by a power amplifier (AE Techron 7224) in the current control (CC) mode. This transient is still longer than that in our previous smaller hand-MRI system, 22 ms [24]. Thus there is loss of the signal due to the extra delay of 38 ms, but it is compensated for by stronger polarization. Unfortunately, the amplifier, while reducing the transient time, introduced a slow current drift associated with the heating of the Bm coil. This drift was minimized by measures discussed in the next section.

III. Experimental results and discussion

Many aspects of our MRI system and imaging method were explained in Ref. [24]. In the current work we focused on demonstration of imaging a larger object – the adjacent parts of the forearm and the wrist. This imaging object was chosen due to easily identifiable features and fairly large bones of the forearm near the wrist. The images would help to project quality to images of other parts of extremities. One question of interest is if the quality of the limited-resolution ULF MRI is better for larger body structures. The system could be also used for imaging animals and tissues of larger sizes than in previous work.

The sequence used is described in Fig. 1. Imaging parameters were as follows: the horizontal direction resolution (pixel size) – 3mm, the vertical direction resolution – 1.5 mm, the slice thickness – 10 mm; the gradient strengths: in the readout direction 73 Hz/cm (readout window 100 ms with appodization), the horizontal phase encoding direction ± 64 Hz/cm maximum, the slice selection direction ± 35 Hz/cm. The effective phase encoding duration was 27 ms. The phase encoding gradients lasted 5 ms after the echo pulse to remove parasitic excitation by imperfect echo pulses, which occurred due to non-uniformity of the RF coil field.

We found that there were drifts in the experiment that deteriorated resolution over long scan times. To reduce the effect of the drifts, the imaging experiments were started after about 45 minutes from turning on the Bm current. However, Bp coil heating introduced additional drift during the scan that was difficult to remove. To minimize artifacts from the drift we took multiple images for shorter times and added them with optimized pixel shifts in horizontal and vertical directions. For images presented here, we acquired 4 separate images, each with 3-minute acquisition time. Fig. 2 shows a comparison of a single scan with the composite image of 4 scans (12 minute of total acquisition time). As expected, the composite image reveals much better quality than a single image. This method can remedy various effects of slow drifts and is easy to implement. The only requirement is sufficient SNR in a single scan; otherwise, it can be difficult to overlap the images correctly. We did find that the SNR of successive 3-minute images became worse with time, which we attributed to the heating of Bp coil leading to the reduction in Bp current and hence Bp field.

It is useful, since ULF-MRI has been shown to give higher contrast [1], to discuss the concept of object visibility, which is the measure of tissue discrimination and the detectability of anomalies. In Ref. [26] the visibility is defined as

$$\nu_{AB}=CNR_{AB}\sqrt{n_{voxel}}=(SNR_A-SNR_B)\sqrt{n_{voxel}} \quad (1)$$

where CNR_{AB} is the contrast-to-noise ratio, n_{voxel} is the number of voxels of the tissue, and $SNR_{A,B}$ the voxel SNR of tissues A and B. The visibility is proportional to the square root of the number of pixels in the object and to the difference in the SNR between the object of interest (A) and surrounding tissue (B). If contrast is large, the visibility of the object is approximately $SNR_A\sqrt{n_{voxel}}$ (we assumed that T_1 of tissue A is longer) but if the contrast is small the visibility can be much smaller than this. Thus ULF MRI, which provides high contrast and significant T_1 weighting, can lead to high visibility of the anomalous tissues even for relatively low SNR:

$$\nu_{AB}\infty\exp(-t/T_{1A})-\exp(-t/T_{1B})\approx t(T_{1A}-T_{1B})/T_{1A}T_{1B} \quad (2)$$

The visibility also increases for larger objects to become detectable even with low-sensitivity ULF MRI. Fine tuning can be required for specific T_1 and T_2 properties of tissues and anomalies to optimize the visibility. Thus for applications, it might be necessary to obtain two images, one for showing overall anatomical structure and the second tuned to provide highest visibility of anomalies. The second-type image can be only bright spots revealing the anomaly which can be coordinated with the general anatomical image.

IV. Conclusion

We have modified our previous non-cryogenic ultra-low MRI system to accommodate larger imaging objects and demonstrated image quality for the adjacent parts of the wrist and the forearm. The system now can be of interest to applications of wrist, arm, elbow imaging,

animal imaging and for imaging of other objects. In order to compensate for the reduced sensitivity of the larger receiver coil we increased the pre-polarization field to 2 kG. This introduced the problem of transients, which was partially solved by using a current controlled power amplifier. We experienced slow drifts of the field in the system that prevented improvement of image quality in longer scans. This problem was solved by using short full scans and superimposing images with optimized shifts. The current experiments serve as a preliminary step for implementing a head MRI system, which has similar transient problems and instabilities. The current system can be useful for research on diseases of the hand, forearm, elbow, and arm and for research on rats and comparable in size animals. In particular, it is known that ultra-low field provides high relaxation contrast and can find applications in cancer detection.

Acknowledgments

This work is sponsored by NIH grant 5 R01 EB009355.

References

1. Lee SK, Mößle M, Myers W, Kelso N, Trabesinger AH, Pines A, Clarke J. SQUID-Detected MRI at 132 μT with T_1-Weighted Contrast Established at 10 μT–300 mT. Magn Res in Med. 2005; 53:9–14.
2. Venook RD, Matter NI, Ramachandran M, Ungersma SE, Gold GE, Giori NJ, Macovski A, Scott GC, Conolly SM. Prepolarized Magnetic Resonance Imaging around Metal Orthopedic Implants. Magn Res in Med. 2006; 56:177–186.
3. Martí-Bonmatí L, Kormano M. MR equipment acquisition strategies: low-field or high field scanners. Eur Radiol. 1997; 7(Suppl.5):S263–S268.
4. Hayashi N, et al. Utilization of Low-Field MR Scanners. Magn Res in Med Sciences. 2004; 3:27–38.
5. Orrison WW Jr, Stimac GK, Stevens EA, et al. Comparison of CT, low-field-strength MR imaging, and high-field-strength MR imaging. Radiology. 1991; 181:121–127. [PubMed: 1887020]
6. Merl T, Scholz M, Gerhardt P, et al. Results of a prospective multicenter study for evaluation of the diagnostic quality of open whole-body low-field MRI unit. A comparison with high-field by the applicable gold standard. Eur J Radiol. 1999; 30:43–53. [PubMed: 10389012]
7. Allmann KH, Walter O, Laubenberger J, et al. Magnetic resonance diagnosis of the interior labrum and capsule. Effect of field strength on efficacy. Invest Radiol. 1998; 33:415–420. [PubMed: 9659595]
8. Dubrulle F, Delomez J, Kiaei A, et al. Mass screening for retrocochlear disorders: low-field-strength (0.2-T) versus high-field-strength (1.5-T) MR imaging. AJNR. 2002; 23:918–923. [PubMed: 12063216]
9. Bryant RG, Mendelson DA, Lester CC. The Magnetic Field Dependence of Proton Spin Relaxation in Tissues. Magn Res in Med. 1991; 21:117–126.
10. Matter NI, Scott GC, Venook RD, Ungersma SE, Grafendorfer T, Macovski A, Conolly S. Three-dimensional prepolarized magnetic resonance imaging using rapid acquisition with relaxation enhancement. Magn Reson in Medicine. 2006; 56:1085–1095.
11. Macovski A. MRI: A Charmed Past and an Exciting Future. JMRI. 2009; 30:919–923. [PubMed: 19856404]
12. Venook, Ross D., et al. Prepolarized Magnetic Resonance Imaging around Metal Orthopedic Implants. Magn Res in Med. 2006; 56:177–186.
13. Ungersma, Sharon E., et al. Magnetic Resonance Imaging with $T1$ Dispersion Contrast. Magn Res in Med. 2006; 55:1362–1371.
14. McDermott R, Lee SK, ten Haken B, Trabesinger AH, Pines A, Clarke J. Microtesla MRI with a superconducting quantum interference device. Proc Natl Acad Sci USA. 2004; 101:7857–7861. [PubMed: 15141077]

15. Zotev VS, Volegov PL, Matlashov AN, Espy MA, Mosher JC, Kraus RH Jr. Parallel MRI at microtesla fields. JMR. 2008; 192:197–208. [PubMed: 18328753]
16. Espy M, Flynn M, Gomez J, Hanson C, Kraus R, Magnelind P, Maskaly K, Matlashov A, Newman S, Owens T, Peters M, Sandin H, Savukov I, Schultz L, Urbaitis A, Volegov P, Zotev V. Ultra-low-field MRI for the detection of liquid Explosives. Supercond Sci Technol. 2010:034023.
17. Zotev VS, Matlashov AN, Volegov PL, Savukov IM, Espy MA, Mosher JC, Gomez JJ, Kraus RH Jr. Microtesla MRI of the human brain combined with MEG. JMR. 2008; 194:115–120. [PubMed: 18619876]
18. Savukov IM, Romalis MV. NMR detection with an atomic magnetometer. Phys Rev Lett. 2005; 94:123001. [PubMed: 15903914]
19. Xu S, et al. Magnetic resonance imaging with an atomic magnetometer. PNAS. 2006; 103:12668–12671. [PubMed: 16885210]
20. Savukov IM, Zotev VS, Volegov PL, Espy MA, Matlashov AN, Gomez JJ, Krauss RH Jr. MRI with an atomic magnetometer suitable for practical imaging applications. JMR. 2009; 199:188–191. [PubMed: 19435672]
21. Lee SK, Sauer KL, Seltzer SJ, Alem O, Romalis MV. Subfemtotesla radio-frequency atomic magnetometer for detection of nuclear quadrupole resonance. Appl Phys Lett. 2006; 89:214106.
22. Savukov IM, Seltzer SJ, Romalis MV. Detection of NMR signals with a radio-frequency atomic magnetometer. JMR. 2007; 185:214. [PubMed: 17208476]
23. Lee SK, Romalis MV. Calculation of magnetic field noise from high-permeability magnetic shields and conducting objects with simple geometry. J Appl Phys. 2008; 103:084904.
24. Savukov I, Karaulanov T, Castro A, Volegov P, Matlashov A, Urbatis A, Gomez J, Espy M. Non-cryogenic anatomical imaging in ultra-low field regime: Hand MRI demonstration. JMR. 2011; 211:101–108. [PubMed: 21700482]
25. Teh J, Whiteley G. MRI of soft tissue masses of the hand and wrist. Brit J of Radiology. 2007; 80:47–63.
26. Haacke, EM.; Brown, RW.; Thompson, MR.; Venkatesan, R. Magnetic Resonance Imaging Physical Principles and Sequence Design. John Wiley & Sons, Inc; 1999.

Highlights

- We built an inexpensive portable non-cryogenic MRI scanner for medical imaging
- We demonstrated the magnetic resonance images of wrist-forearm area
- The scanner can be applicable to medical diagnostics and research
- The new setup features much larger prepolarization coil and imaging volume

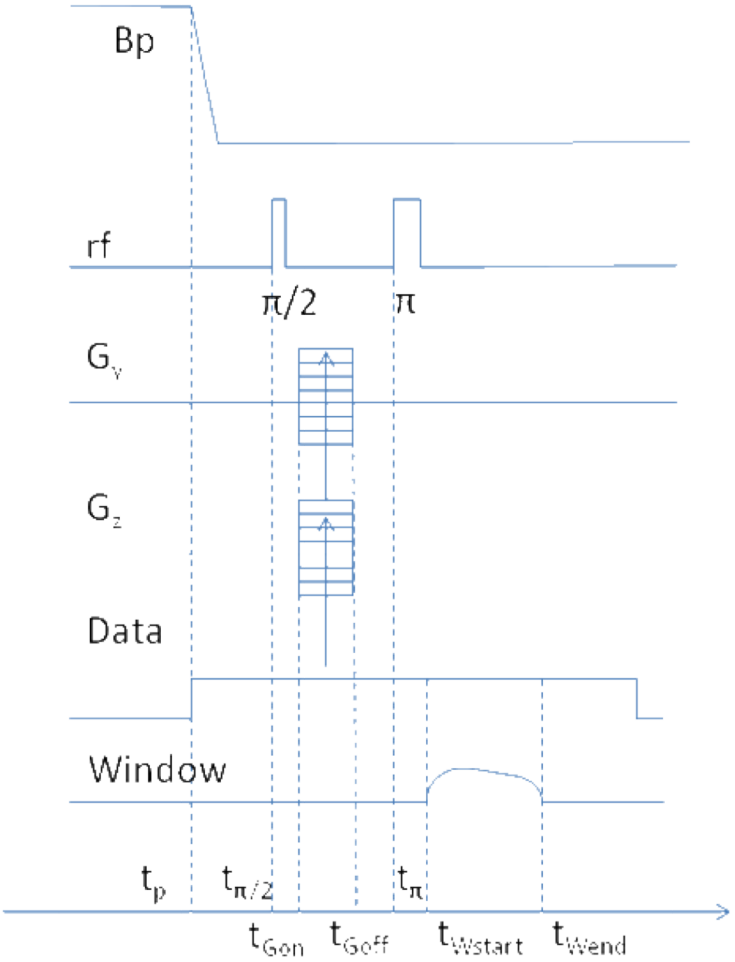

Fig. 1.

Pulse sequence: t_p=350 ms, $t_{\pi/2}=t_p$+69 ms, $t_\pi=t_{\pi/2}$+32 ms, $t_{Gon}=t_p$+68 ms, t_{Goff}= t_{Gon} +37 ms, t_{Wstart}= t_p +120 ms, $t_{W.end}$= t_{Wstart}+100 ms. Repetition time is 600 ms.

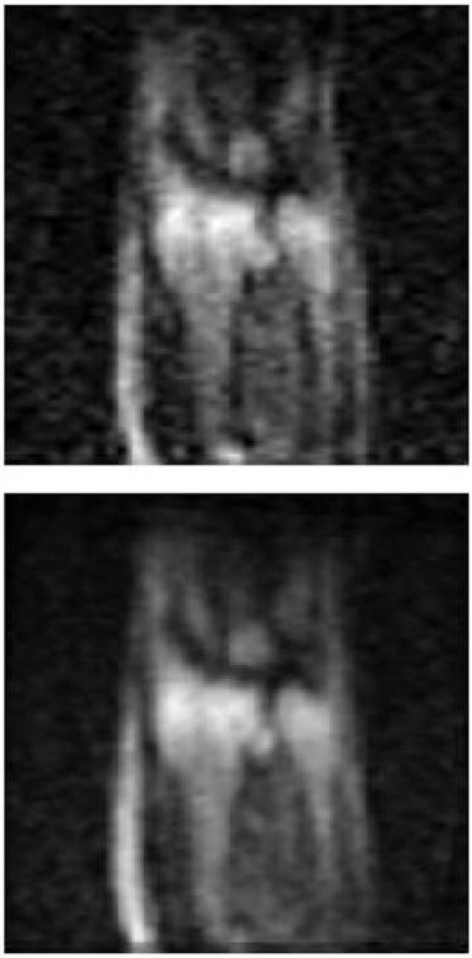

Fig. 2.
ULF MRI of the adjacent areas of the wrist and the forearm. The top image is obtained in 3 minutes. The bottom image is obtained by combining four 3-minute images with optimized shifts and brightness adjustments.